

Chapter 2

Spatial variations in field data

This chapter illustrates strong spatial variability in a multi-component surface seismic data set. One of the simplest methods for analyzing variability is looking at the total or partial energy in a seismic trace. This value is a good indicator of spatial variability throughout the entire data set. I show, using a nine-component land and a conventional marine data set, that the variability in the seismic land data is greater than for a marine dataset, because wave propagation on land is complicated by the presence of near surface heterogeneities, which are virtually absent in marine data. Such near-surface properties dominate the transfer of energy to and from the earth for multi-component sources and receivers.

2.1 A nine-component land dataset

This section analyses a nine-component data set that was recorded with equal and constant source-receiver spacing in a split spread geometry. I applied a despiking algorithm to remove unreasonable samples that were clearly not generated by the earth's response.

Figure 2.1 shows a typical nine-component shot gather with 200 channels recorded per single shot. This data set was collected within an active production area. Some surface locations are not accessible and thus show up as zero traces. The shot gathers were linearly muted to remove direct, refracted and surface waves; a t^2 gain was applied to even out the signal level for later arrival times. Within the gather one sees nearly monochromatic energy on some individual locations, which likely is caused by nearby drilling activity. Another lower frequency band-limited signal is visible particularly on the

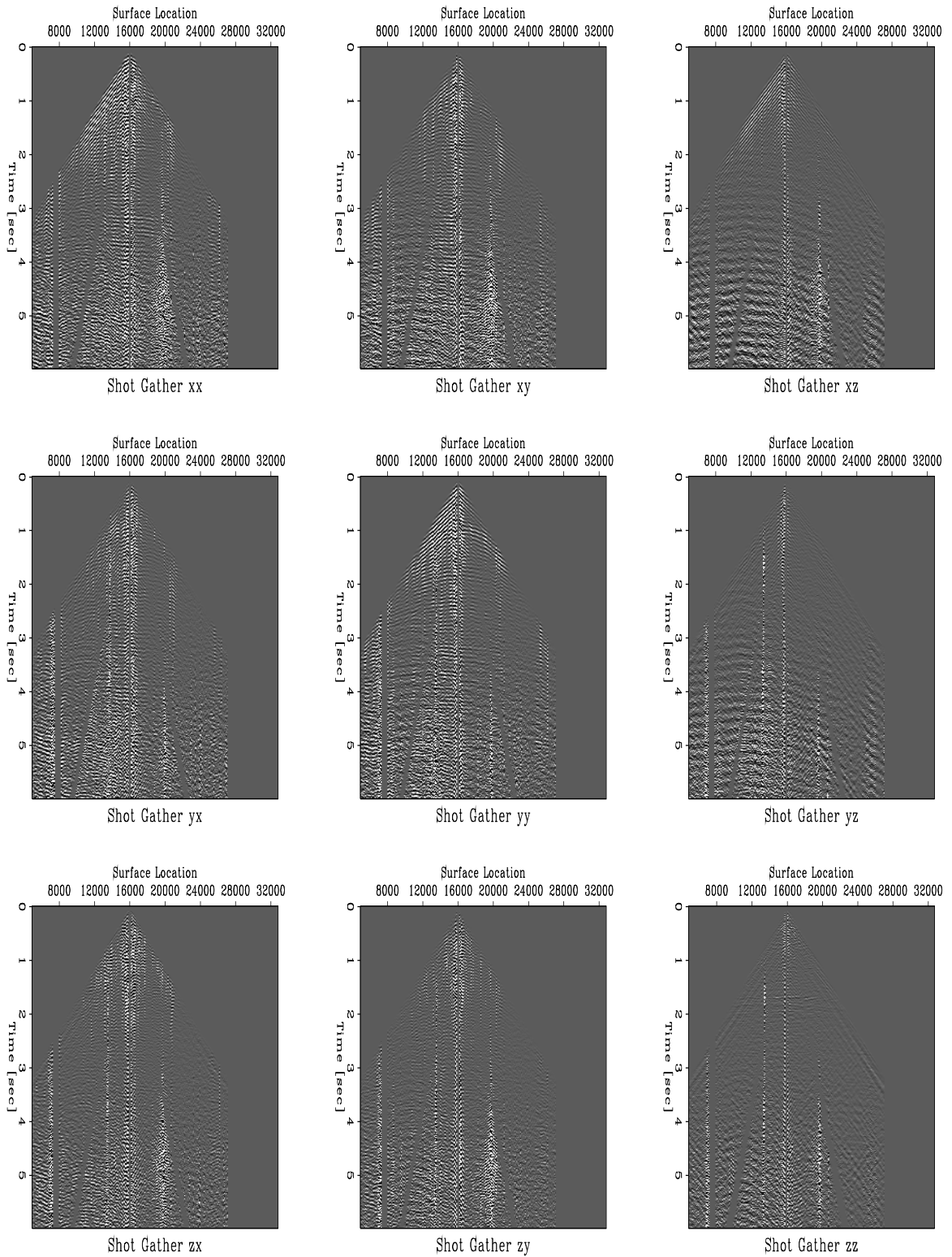


FIG. 2.1. One shot gather of a nine-component dataset. A linear mute was applied to remove supercritical reflections at early times. Amplitudes for all components are relative to the Xx component with a t^2 gain applied. The arrangement of components follows the matrix in equation (1.1). `var9c-allmgather` [R]



FIG. 2.2. One common offset section of a 9 component dataset. A linear mute was applied to remove supercritical reflections at early times. Amplitudes for all components are relative to the Xx component with a t^2 gain applied. The arrangement of components follows the matrix in equation (1.1). `var9c-allcoff` [R]

Xz and Yz components. The source of such a signal could be a pump site in close proximity because of the steady low-frequency character that is picked up primarily by z receiver components and because of the signal's amplitude increase with time. The subsurface structure is not complex in this area, as one can see in Figure 2.2. The primary targets are tar-and gas-sands embedded in a relatively flat subsurface. Figure 2.2 shows near offset sections of all nine components with various reflection events between 0.8 and 2 seconds, extending across all CMP locations; the entire recording time was 6 seconds. These events are visible in various ways on the different component sections. Their strength depends on the particular wave type and on the component that is recording the signal. Another event of limited spatial extent is visible at later times; between 3 and 3.5 seconds its amplitude stands out more strongly on the Xx and Yy component than any other component. Additionally, surface-location dependent effects can be seen on several traces, where suddenly the amplitude is anomalously high or low for nearly the entire trace. From this preprocessed data I computed the total energy, according to the integral

$$E(\mathbf{x}_s, \mathbf{x}_r) \equiv \int_{t_{min}}^{t_{max}} D(\mathbf{x}_s, \mathbf{x}_r, t)^2 dt = \int_{t_{min}}^{t_{max}} [S(\mathbf{x}_s) \cdot G(\mathbf{x}_s, \mathbf{x}_r, t) \cdot R(\mathbf{x}_r)]^2 dt \quad (2.1)$$

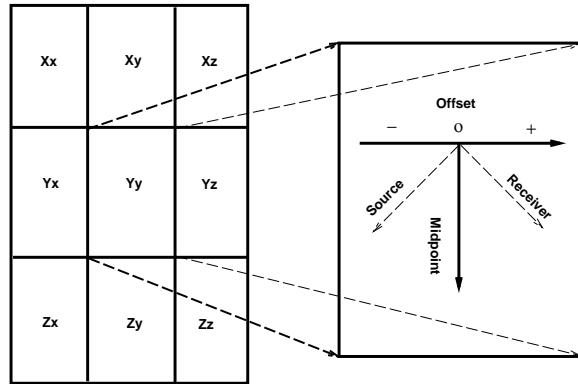
where E is the total energy and D the actual data. In this model equation S and R are operators that apply source and receiver effects and G denotes the subsurface Green's function that, in this case, describes a wave field response from a nearly flat subsurface structure. I assume that the subsurface reflects uniformly and source and receiver effects can be represented as scalar quantities. Each trace in the data set is then represented as a single sample value. Figure 2.4 shows the plot of total energy in each trace in the source-receiver-coordinate system. The figure consists of a 3×3 matrix of energy plots. The top row is the energy for the X source component recorded into x, y, z receiver components (from left to right); likewise, the middle row is characteristic for the Y and the bottom row for the Z source component.

These figures are analogous to Kjartansson's energy plots (1979) for scalar pressure data. All nine components are plotted consistently, as illustrated in Figure 2.3, so that the midpoint axis extends vertically in the middle of the sub-plot; midpoint locations are increasing from top to bottom. The offset axis is oriented perpendicular to the midpoint axis, maximum negative offset is on the left side, and maximum positive offset is on the right side of the sub-plot. Figures 2.4 and 2.5 plot the trace energy using a logarithmic scale with a dynamic range of 1:1000. Several features are common on all plots in Figures

2.4 and 2.5: several missing source locations traverse the plots diagonally from the upper left to lower right side; a missing receiver traverses the plot from the upper right to lower left; those locations display zero energy. Missing zero offset traces represent the midpoint axis in the middle of the sub-plots; they extend down vertically and are surrounded by a few extremely high energy traces. The leftmost column of plots, associated with the z component receiver, has consistently lower energy levels than the other two horizontal receiver components x, y . There are high amplitude values that do not follow a particular receiver or source and which are visible on all components, that is, those indicating high-energy noise sources influencing only the immediate neighborhood over a short period of time.

Besides those common features, Figure 2.4 shows differences in energy levels either aligned with certain sources or certain receivers. Energy levels exhibit low amplitude regions in the lower part of the sub-plots and especially on the Zz component. In Figure 2.4, this feature is still visible, but less pronounced; Figure 2.4 displays the energy in a data window from 3 to 4 seconds. The energy in this window is likely not to be dominated by energetic surface waves and strong reflections from the near subsurface, as is the case in Figure 2.4. On the windowed energy plots, the pattern of source and receiver variations seems nearly independent, with both kinds of variation standing out distinctly.

FIG. 2.3. Each component's sub-plot displays midpoint and offset space with offset increasing from left to right and zero offset in the middle. The midpoint axis extends down vertically. var9c-arrange [NR]



The standard Kjartansson model of lateral variations serves well to explain simplified earth models; however, usually it does not include a source and receiver model. Sources and receivers rather are assumed to respond isotropically and uniform. Examining the energy distribution in this nine-component land data set, one realizes that these huge

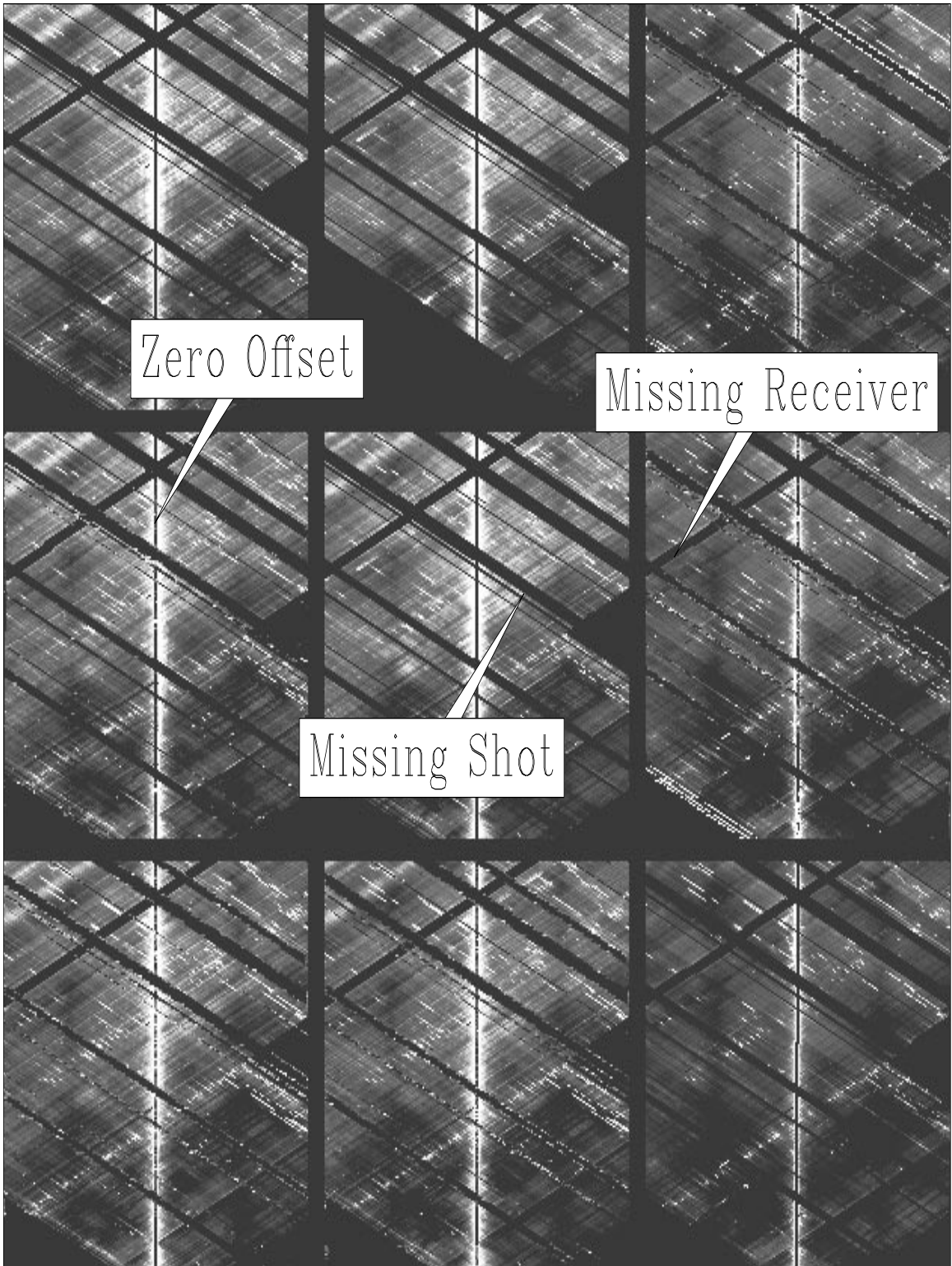


FIG. 2.4. The energy of all nine components is plotted in midpoint-offset space. A logarithmic scale with a range from 1:1000 is used to show energy values. var9c-logenergy
[R]

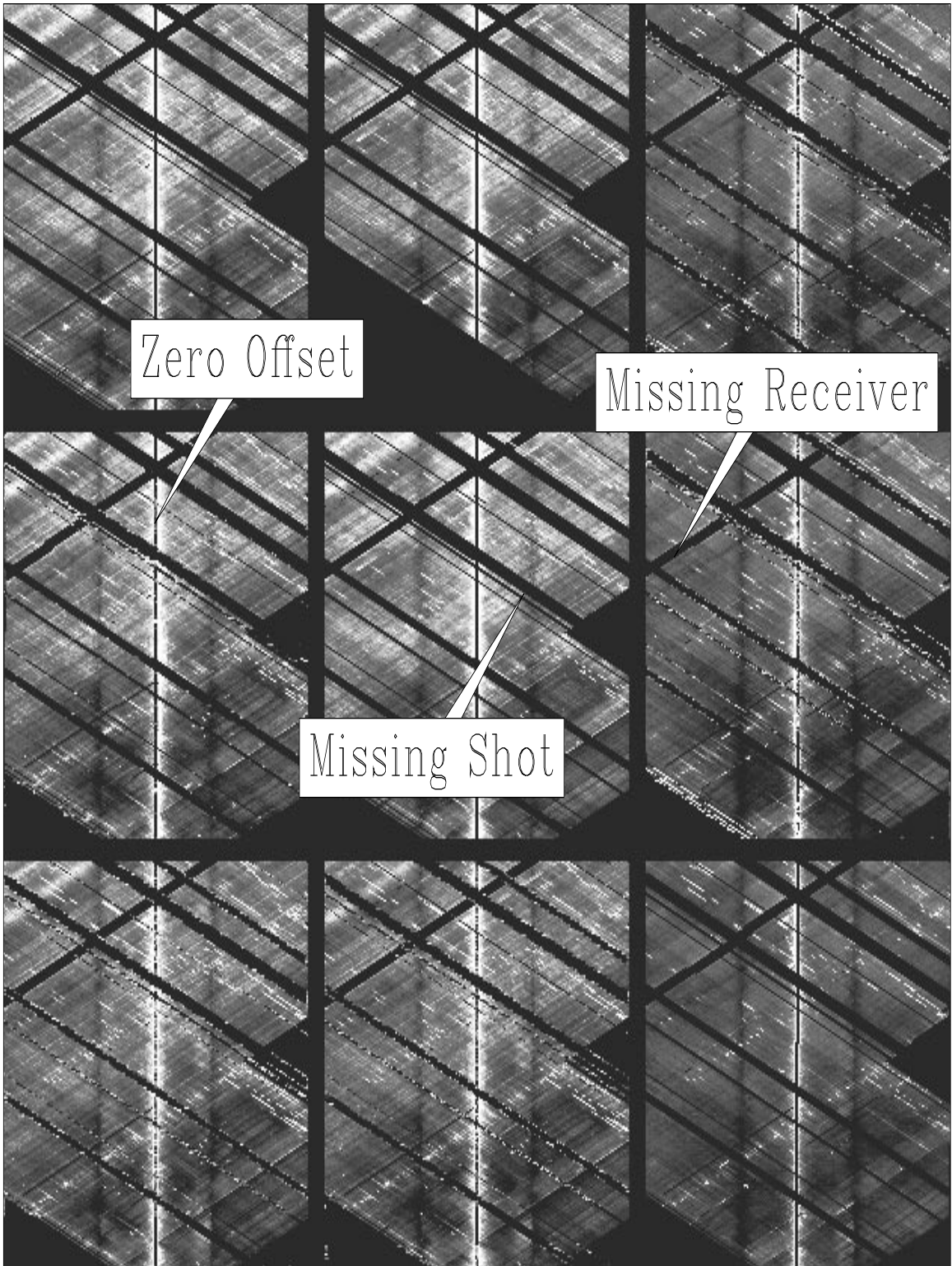


FIG. 2.5. The energy of all nine components are plotted in midpoint-offset space for a time window between 3-4 seconds two-way travelttime. A logarithmic scale with a range from 1:1000 is used to show energy values. `var9c-logwenergy` [R]

differences in energy are produced not by the earth's reflection response, but are dominated by how strongly sources radiate elastic energy into the ground and how well receivers are able to pick it up. Kjartansson's model can be augmented to incorporate effects of source and receiver radiation effects. Figure 2.6 depicts a reflector at a certain depth z that extends along the whole subsurface with more or less variability. Each receiver r and source s possesses a certain radiation characteristic. The exact behavior is determined by the type of component in contact with the earth's surface. Heterogeneities close to the source or receiver influence the characteristic, so that from far distances an effective radiation pattern is observed.

For a point source with an isotropic radiation pattern that illuminates the target uniformly, one expects a smooth amplitude variation with offset (AVO). In contrast, a single component force in contact with the earth's free surface is capable of producing strong non-uniform patterns.

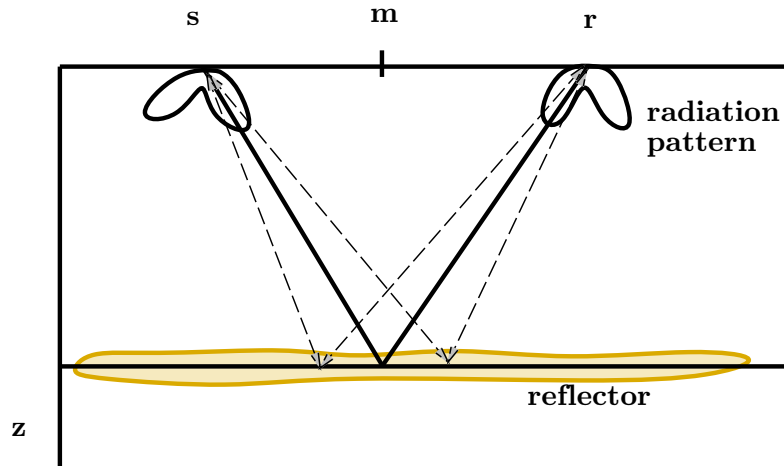


FIG. 2.6. Kjartansson's model is augmented by including source and receiver radiation patterns. var9c-mkkjidea [NR]

Horizontal and vertical source and receiver components produce different radiation characteristics. According to Figure 2.6, a reflector produces a stronger effect in the data, if it is either illuminated more strongly by a source or if the receiver is more directed towards picking up weaker signals from the reflector. In Figure 2.6, the solid ray path illustrates this; the ray, either on its path down or on its path up, is within a high gain lobe of the radiation pattern. For a theoretical Z source, the radiation pattern is rotationally

invariant about the vertical axis and thus should produce consistent effects regardless of the orientation of the other component's pattern. The pattern for both the x, y horizontal components should be similar, but they are not rotationally invariant about the vertical axis. Thus, their source and receiver patterns neither generate nor record signals in an optimal way from that subsurface reflector; however, they may be tuned to some other reflector, as Figure 2.2 shows for the event in the middle of the section at around 3 seconds.

Such a general look at energy plots gives a rough indication of spatial variability. Another interesting point is the variability among source and receiver components. Theoretically, one would expect consistent behavior through all receiver components for a given source component. The same holds true for all source components, given a certain receiver component. But that theoretical expectation is not met, as Figure 2.4 and 2.5 illustrate. Although there is some consistency row-wise and column-wise in general features, the data indicate a huge amount of variability. This is an example of nine-component land seismic data, whose behavior contrasts with typical marine data, shown in the next section.

2.2 A marine dataset

Marine data behave differently from land data as far as source and receiver behavior is concerned. Sources and receivers are more or less immersed in a medium that shows little heterogeneity and variability. A complicated heterogeneous near surface, as present in land data, is absent. Figure 2.7 depict four neighboring CMP gathers out of the prestack data set. I compute total energy levels in the prestack data set after applying a t^2 gain to all traces. Figure 2.8 shows energy variations in midpoint and offset space. As one can recognize, variability in sources and receivers are less pronounced than those of the land data in Figure 2.5. This plot is represented in midpoint and offset space in the same way as Kjartansson's original observations. In the energy plot, streaks of different amplitudes at an oblique angle for all offsets are associated with one particular receiver, while streaks with an opposite slope are associated with a particular source location. Near zero offset a few high amplitude peaks are observable, which indicates the presence of subsurface reflection anomalies that are confined to a few CMP locations. That reflected energy is produced by some subsurface structure and not by source or receiver effects.

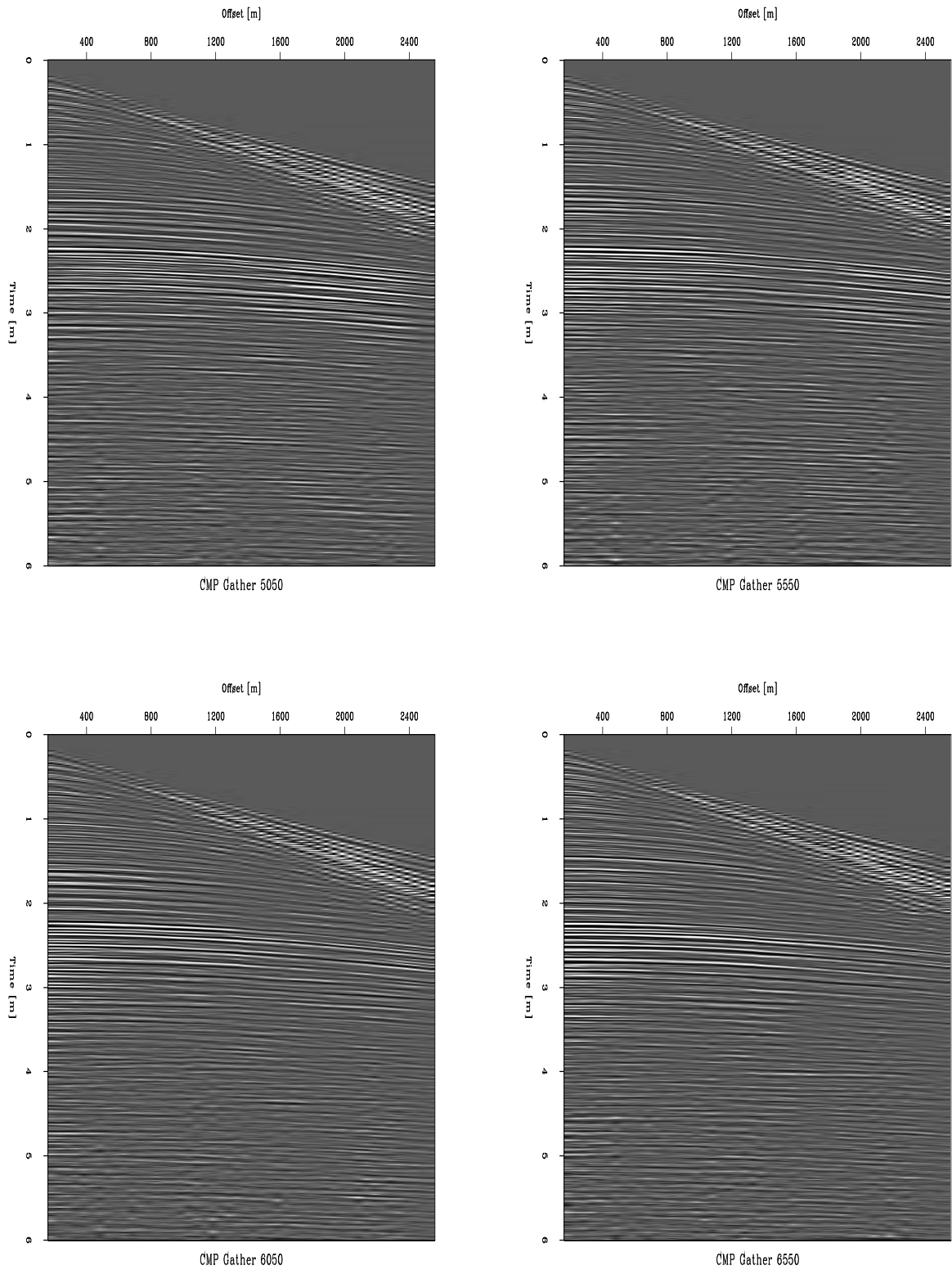


FIG. 2.7. The four marine CMP gathers are comparable in their source and receiver variations. The target of interest is in the zone around 2 seconds two-way travelttime. The gathers are spaced 500 meters apart, and a t^2 gain applied to the sections. var9c-fourcdp
[R]

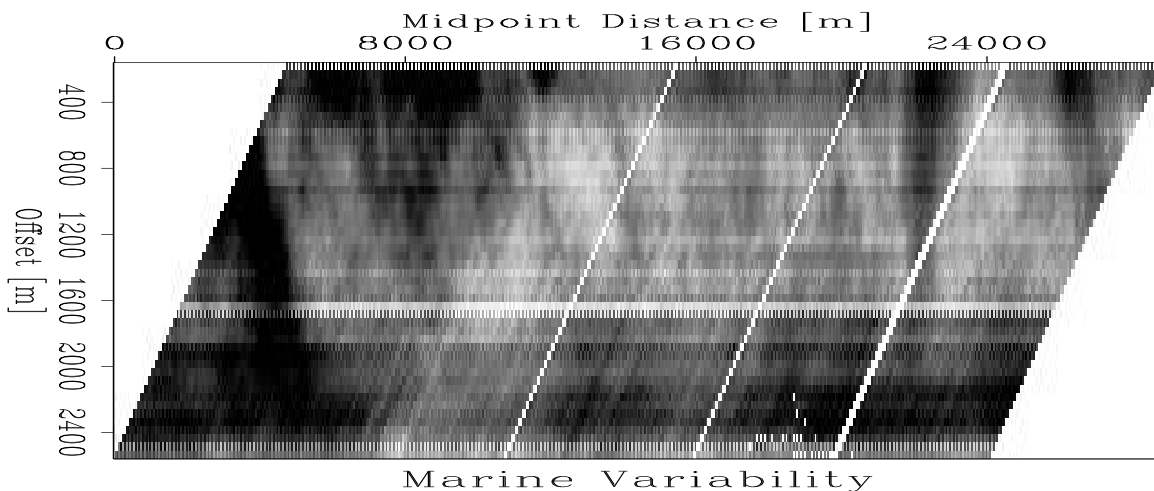


FIG. 2.8. For each trace in a marine dataset, the total energy is plotted in midpoint-offset space. The pattern of variability is mostly due to small source variations and, to a lesser degree, to hydrophone variations. `var9c-marine` [R]

2.3 Summary

In this chapter I compared two data sets in their overall reflection energy behavior. One data set was collected on land and consists of multi-component recordings; the other data set was collected in a marine environment and consisted of pressure recordings. The land source was a multi-component device, while the marine source was a conventional airgun. When one compares energy plots for the different experiments, the difference that one observes in energy variability is huge. That is an indication that the nine-component land data set has a large degree of signal variability in general. One reason for this variability is that multi-component land source and receiver interact with a more heterogeneous earth subsurface, while marine sources and receivers are immersed in a more homogeneous environment. Another reason is that for land sources, it is usually harder to generate consistent identical behavior.